



Light-stimulated cargo release from a core–shell structured nanocomposite for site-specific delivery



Yun Cai^a, Li Ling^a, Xiaofang Li^a, Meng Chen^b, Likai Su^{a,*}

^a Department of Neurology, Affiliated Hospital of Hebei University, Baoding 071000, PR China

^b Department of Rheumatology, Affiliated Hospital of Hebei University, Baoding 071000, PR China

ARTICLE INFO

Article history:

Received 14 November 2014

Received in revised form

30 January 2015

Accepted 24 February 2015

Available online 5 March 2015

Keywords:

Site-specific delivery

Core–shell structure

Magnetic feature

Light switch

ABSTRACT

This paper reported a core–shell structured site-specific delivery system with a light switch triggered by low energy light ($\lambda = 510$ nm). Its core was composed of supermagnetic Fe_3O_4 nanoparticles for magnetic guiding and targeting. Its outer shell consisted of mesoporous silica molecular sieve MCM-41 which offered highly ordered hexagonal tunnels for cargo capacity. A light switch N1-(4aH-cyclopenta[1,2-b:5,4-b']dipyridin-5(5aH)-ylidene)benzene-1,4-diamine (CBD) was covalently grafted into these hexagonal tunnels, serving as light stimuli acceptor with loading content of 1.1 $\mu\text{M/g}$. This composite was fully characterized and confirmed by SEM, TEM, XRD patterns, N_2 adsorption/desorption, thermogravimetric analysis, IR, UV–vis absorption and emission spectra. Experimental data suggested that this composite had a core as wide as 150 nm and could be magnetically guided to specific sites. Its hexagonal tunnels were as long as 180 nm. Upon light stimuli of “on” and “off” states, controllable release was observed with short release time of ~ 900 s (90% capacity).

© 2015 Elsevier Inc. All rights reserved.

1. Introduction

For their potential application in drug transportation field, site-specific delivery systems have been insensitively explored and reported [1,2]. An ideal delivery system is supposed to release therapeutic drug level at specific tissues, organs or even cellular structures. Before reaching target organs or tissues, no cargo molecules should be released since some of them are generally toxic and harmful to normal organs as well as to abnormal ones. In addition, a perfect delivery system should be highly stable to experience various physiological conditions, holding cargo molecules tightly and safely. So far, some candidates have been proposed. However, few of them can meet all above requirements well [3,4]. For example, biodegradable polymers have been reported as a delayed release supporting host for drug molecules. In this case, their release process is controlled by their hydrolysis-induced erosion [3]. Their drawback localizes at the fact that such release process happens immediately upon dispersion in water, which makes them unsuitable for toxic drug delivery such as antitumor medicament. What's more, it is nearly impossible to request a site-specific release from them. Thus, it is needed to explore and develop smart delivery systems with both controllable release and site-specific character.

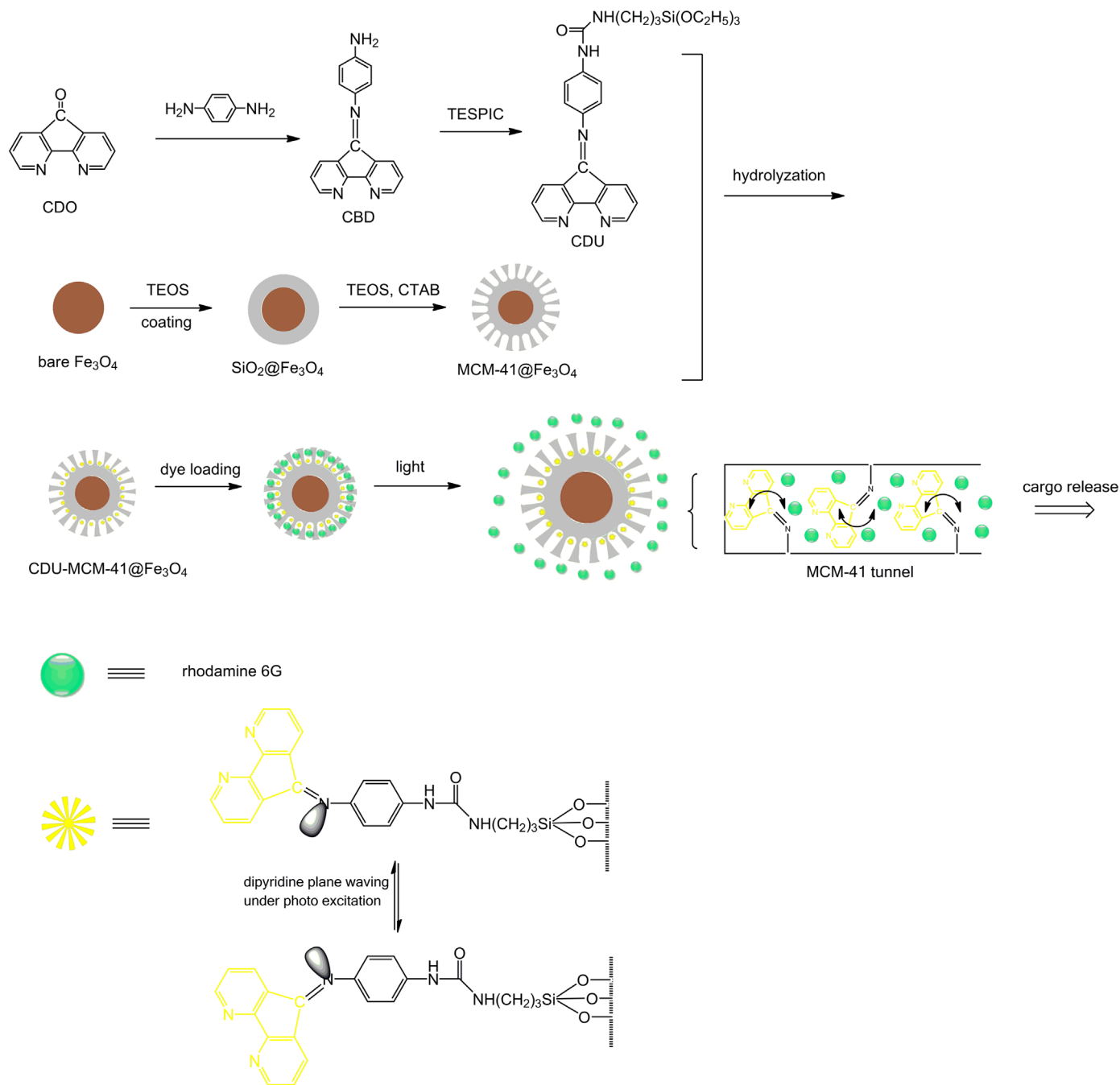
Core–shell structured nanocomposites are then proposed to meet above requirements since they can combine advantages of each component without compromising individual character [4–7]. A representative core–shell structured site-specific delivery system usually has a magnetic core which is responsible for magnetic guiding [8,9]. Its outer shell is usually composed of mesoporous or amorphous silicates which are here used to support cargo molecules and other functional components.

Aiming at controllable and active release, stimulus-sensitive switches should be embedded into such core–shell structured nanocomposites, such as light, pH, competitive binding, enzymes and chemical reactions [10–12]. Of all these candidates, light switch has been considered promising owing to its virtue of noninvasive therapy, which makes it free of biological interferences, giving instant and controllable release. Some precursive efforts have tried azobenzene and its derivatives as light switch owing to their trans/cis isomerization and high compatibility with supporting hosts [13,14]. However, these light switches need high energy light peaking at 450 nm which causes severe light damage to live body is nearly impenetrable for live tissues and is nearly impenetrable for live tissues. Thus, core–shell structured site-specific delivery system with light switch triggered by low energy light should be explored and developed.

Guided by above consideration, in this effort, we decide to construct a core–shell structured site-specific delivery system with light switch triggered by low energy light. To achieve this goal, magnetic nanoparticles were used as core, mesoporous silicate

* Corresponding author. Tel.: +86 312 5981036; fax: +86 312 5981036.

E-mail address: zhangdong19992003@163.com (L. Su).



Scheme 1. Synthetic route for CDU and construction strategy for CDU-MCM-41@Fe₃O₄.

MCM-41 was grown onto this core, serving as supporting host. As shown in **Scheme 1**, a light switch derived from 1,10-phenanthroline was grafted into MCM-41 shell so that it could be triggered by low energy light. The resulting nanocomposite was characterized in detail, along with its controllable release character.

2. Experimental details

2.1. General information

Construction route and operating principle of our nanocomposite (denoted as CDU-MCM-41@Fe₃O₄) are shown in **Scheme 1**. Starting compounds, 1,10-phenanthroline, benzene-1,4-diamine, 3-(triethoxysilyl)propyl isocyanate (denoted as TESPIC) and rhodamine 6 G,

were obtained from Aldrich Chemicals Co. and used as received with no purifications. Other chemicals, including NH₃ · H₂O, HCl, NH₄AC, *N,N*-dimethylformamide (DMF), cetyltrimethylammonium bromide (denoted as CTAB, AR grade), tetraethoxysilane (denoted as TEOS), FeCl₃ · 6H₂O, anhydrous sodium acetate, ethylene glycol, *p*-toluene sulfuric acid, *n*-hexane, chloroform, toluene and ethanol, were bought from Tianjin Chemical Company. All organic solvents were purified through standard procedures. Solvent water used in this work was deionized.

Equipments used for sample characterization are listed as follows. NMR, mass and IR spectra were obtained from a Varian INOVA 300 spectrometer, a Agilent 1100MS series/AXIMA CFR MALDI/TOF (matrix assisted laser desorption ionization/time-of-flight) MS (COM-PACT) and a Bruker Vertex 70 FTIR spectrometer (400–4000 cm⁻¹, KBr pellet), respectively. Elemental analysis was finished on a Carlo

Erba 1106 elemental analyzer. Photophysical parameters were measured from a Hitachi F-4500 fluorescence spectrophotometer and a HP 8453 UV–vis–NIR diode array spectrophotometer, respectively. X-ray diffraction (XRD) data were collected by a Rigaku D/Max-Ra X-ray diffractometer ($\lambda = 1.5418 \text{ \AA}$). Sample morphology was measured by scanning electron microscopy (SEM), transmission electron microscopy (TEM) and energy-dispersive analysis of X-ray (EDAX) on a Hitachi S-4800 microscope and a JEM-2010 transmission electron microscope (Japanese JEOL Company). Thermogravimetric analysis (TGA) data were collected through a Perkin-Elmer thermal analyzer. Magnetic feature was explored on a vibrating sample magnetometer (VSM) (Lake Shore Company) at room temperature. Mesoporous structure was confirmed by N_2 adsorption and desorption measurement with a Nova 1000 analyzer at 77 K. Pore size and volume were calculated by Barrett–Joyner–Halenda (BJH) model. Surface area was determined with Brunauer–Emmett–Teller (BET) model. Above operations were finished in the air at room temperature without specifications.

2.2. Synthesis of CBD and CDU

N1-(4aH-cyclopenta[1,2-b:5,4-b']dipyridin-5(5aH)-ylidene)benzene-1,4-diamine (CBD) was synthesized with 4aH-cyclopenta[1,2-b:5,4-b']dipyridin-5(5aH)-one (CDO) and benzene-1,4-diamine as starting compounds. CDO was first prepared following a literature procedure [15]. CDO (10 mmol), benzene-1,4-diamine (12 mmol) and *p*-toluene sulfuric acid (0.1 g) were dissolved in distilled toluene (20 mL) and heated to reflux under N_2 protection. The resulting crude product was collected and recrystallized in MeOH/toluene to give pure CBD as red powder. ^1H NMR (300 MHz, CDCl_3): δ 8.79 (s, 1H, pyridine Ar-H), 8.65 (s, 1H, pyridine Ar-H), 8.25 (s, 2H, pyridine Ar-H), 7.39 (s, 2H, aniline Ar-H), 7.05–6.99 (m, 2H, pyridine Ar-H), 6.80–6.78 (m, 2H, aniline Ar-H), 4.12 (s, 2H, $-\text{NH}_2$). Anal. Calcd for $\text{C}_{17}\text{N}_4\text{H}_{12}$: C, 74.98; H, 4.44; N, 20.58. Found: C, 74.83; H, 4.52; N, 20.64. EI-MS *m/e*: calc. for $\text{C}_{17}\text{N}_4\text{H}_{12}$, 272.1; found, 272.1 [m] $^+$.

1-(4-((4aH-cyclopenta[1,2-b:5,4-b']dipyridin-5(5aH)-ylidene)amino)phenyl)-3-(3-(triethoxysilyl)propyl)urea (CDU) was synthesized with CBD and TESPIC as starting reagents. CBD (5 mmol) was dissolved in TESPIC (25 mL) and treated with ultrasonic bath for 30 min. The solution was then heated to reflux under N_2 protection. After cooling, this solution was dispersed in cold *n*-hexane (100 mL). Crude product was recrystallized from mixed solvent of CHCl_3 :*n*-hexane (V:V = 2:8). ^1H NMR (300 MHz, CDCl_3): δ 12.12 (b, 1H, aniline-(NH)-CO), 11.47 (b, 1H, C-(NH)-CO), 8.78 (s, 1H, pyridine Ar-H), 8.64 (s, 1H, pyridine Ar-H), 8.22 (s, 2H, pyridine Ar-H), 7.37 (s, 2H, aniline Ar-H), 7.06–6.98 (m, 2H, pyridine Ar-H), 6.81–6.76 (m, 2H, aniline Ar-H), 3.80–3.73 (q, 6H, O-(CH_2)-), 3.13–3.10 (m, 2H, N-(CH_2)-C), 1.57–1.53 (m, 2H, C-(CH_2)-C), 1.20–1.15 (t, 9H, $-\text{CH}_3$), 0.68–0.65 (t, 2H, Si-(CH_2)-). Anal. Calcd for $\text{C}_{27}\text{N}_5\text{H}_{33}\text{O}_4\text{Si}$: C, 62.40; H, 6.40; N, 13.48. Found: C, 62.36; H, 6.52; N, 13.54. EI-MS *m/e*: calc. for $\text{C}_{27}\text{N}_5\text{H}_{33}\text{O}_4\text{Si}$, 519.6; found, 519.2 [m] $^+$.

2.3. Preparation of Fe_3O_4 nanoparticles, $\text{SiO}_2@\text{Fe}_3\text{O}_4$ and MCM-41@ Fe_3O_4

Core-shell structured supporting host was prepared using Fe_3O_4 nanoparticles as core, amorphous silica as middle smoothing layer and MCM-41 as outer shell. Fe_3O_4 nanoparticles were first prepared following a classic literature method [16]. Fresh Fe_3O_4 nanoparticles (0.1 g) were then dispersed in mixed solvent of deionized water (10 mL), $\text{NH}_3 \cdot \text{H}_2\text{O}$ (1 mL) and TEOS (0.1 mL). Then this mixture was stirred under N_2 protection at room temperature for 30 min. The resulting sample ($\text{SiO}_2@\text{Fe}_3\text{O}_4$) was collected and carefully washed with ethanol and then dispersed in mixed solution of CTAB (0.3 g), $\text{NH}_3 \cdot \text{H}_2\text{O}$ (1.2 mL) and deionized water (40 mL). This mixture was stirred by a mechanical stirrer for

30 min under N_2 protection. During this time, TEOS (0.8 mL) was dropwise added. The mixture was mechanically stirred at room temperature for 10 h under N_2 protection. Finally, crude product was collected, dispersed in mixed solution of HCl (5 mL) and ethanol (100 mL) and stirred for 24 h to remove template reagent CTAB. The resulting sample was dried in vacuum at 50 °C to give MCM-41@ Fe_3O_4 .

2.4. Construction of CDU-MCM-41@ Fe_3O_4

The final core-shell structured site-specific delivery system CDU-MCM-41@ Fe_3O_4 was constructed by the following procedure [16]. MCM-41@ Fe_3O_4 (0.2 g) and CDU (0.2 g) were dispersed in anhydrous toluene (20 mL) and heated to reflux under N_2 protection for 12 h. After natural cooling, solid product was collected and washed with anhydrous toluene and ethanol to give CDU-MCM-41@ Fe_3O_4 .

2.5. Dye loading and release monitoring

Rhodamine 6 G was first loaded into CDU-MCM-41@ Fe_3O_4 by the following procedure. CDU-MCM-41@ Fe_3O_4 (0.2 g) was soaked in rhodamine 6 G solution (ethanol, 5 $\mu\text{M/L}$) and stirred for 30 h under 510 nm radiation to achieve dye loading equilibrium. Then this rhodamine 6 G-saturated nanocomposite was collected and washed with ethanol until solution became clear. Dye loading content was determined as 1.1 $\mu\text{M/g}$ (against unloaded CDU-MCM-41@ Fe_3O_4) by concentration difference before and after CDU-MCM-41@ Fe_3O_4 loading with UV–vis absorption spectrophotometry. As for controllable release measurement, rhodamine 6 G-saturated CDU-MCM-41@ Fe_3O_4 suspension (10 mg in 5 mL ethanol) was exposed to periodical “on” and “off” light stimuli ($\lambda = 510 \text{ nm}$). Its corresponding emission spectra were recorded meanwhile. To avoid emission interference from rhodamine 6 G in composite tunnels, CDU-MCM-41@ Fe_3O_4 was concentrated at the bottom of sample pool by a magnet so that it could not be excited by excitation light.

3. Results and discussion

3.1. Characterization on CDU-MCM-41@ Fe_3O_4

3.1.1. Design strategy

Design strategy of CDU-MCM-41@ Fe_3O_4 is explained as follows aiming at a clear understanding on each functional component. As a typical core-shell structure, Fe_3O_4 core is obviously applied for magnetic guiding purpose. This magnetic core is coated by amorphous silica so that its surface can be smoothed and covered, minimizing its negative effect to cargo molecules. In addition, this silica shell may decrease magnetic aggregation between Fe_3O_4 nanoparticles, favoring the following MCM-41 growth procedure. In this effort, MCM-41, a representative mesoporous silica molecular sieve, serves as the supporting host for cargo molecules owing to its big surface-area-to-volume ratio and highly ordered hexagonal tunnels which are positive for cargo adsorption and transportation [17]. Aiming at controllable release, a light switch CDU derived from 1,10-phenanthroline was covalently embedded into MCM-41 channels, avoiding light switch leakage. A C=N bond and a large conjugation plane exist in CDU so that its trans/cis isomerization could be triggered by low energy light. An organic dye rhodamine 6 G was selected as cargo owing to its spectral character. By monitoring rhodamine 6 G spectral character, controllable release character of CDU-MCM-41@ Fe_3O_4 can be evaluated.

3.1.2. Morphology and magnetic feature

CDU-MCM-41@Fe₃O₄ morphology can be first evaluated from its SEM image shown in Fig. 1. Those for Fe₃O₄ nanoparticles, SiO₂@Fe₃O₄ and MCM-41@Fe₃O₄ are presented in Fig. 1 for comparison. Fe₃O₄ nanoparticles are generally spherical with mean diameter of 150 nm. They tend to aggregate together owing to their magnetic nature. There are multiple humps on their surface, showing coarse surface. After silica coating procedure, SiO₂@Fe₃O₄ increases its diameter to 200 nm with its surface greatly smoothed. From its TEM image shown in Fig. 1, this core-shell structure can be confirmed. Magnetic aggregation between them, however, is still obvious. As for MCM-41@Fe₃O₄, silica molecular sieve growth further increases its mean diameter to 550 nm with smooth and porous surface. MCM-41 shell thickness can be calculated as 180 nm, as suggested by its TEM image. These hexagonal tunnels are longer than literature values and can offer a large capacity for cargo molecules [14,16]. After light switch loading procedure, CDU-MCM-41@Fe₃O₄ mean diameter is nearly identical to that of MCM-41@Fe₃O₄, suggesting that these light switch molecules may be grafted

into MCM-41 tunnels instead of MCM-41@Fe₃O₄ surface, which will be later proved.

Hysteresis loops of Fe₃O₄ nanoparticles, SiO₂@Fe₃O₄, MCM-41@Fe₃O₄ and CDU-MCM-41@Fe₃O₄ are presented in Fig. 2. All these samples are supermagnetic ones without any coercivity values. Saturation value for Fe₃O₄ nanoparticles is determined as 82.6 emu/g, which is comparable to literature values [9,14,16]. After a series of modification procedures, saturation values are determined as 75.7 emu/g for SiO₂@Fe₃O₄, 60.5 emu/g for MCM-41@Fe₃O₄ and 57.7 emu/g for CDU-MCM-41@Fe₃O₄, respectively. These decreased values compared to saturation value of Fe₃O₄ nanoparticles can be attributed to their decreased Fe₃O₄ weight ratios. Owing to its hydrophilic surface and supermagnetic nature, CDU-MCM-41@Fe₃O₄ can be easily dispersed in water, forming a stable suspension, as shown by the inset of Fig. 2. In the presence of external magnetic field, CDU-MCM-41@Fe₃O₄ can be magnetically guided to specific places, meeting site-specific delivery requirements.

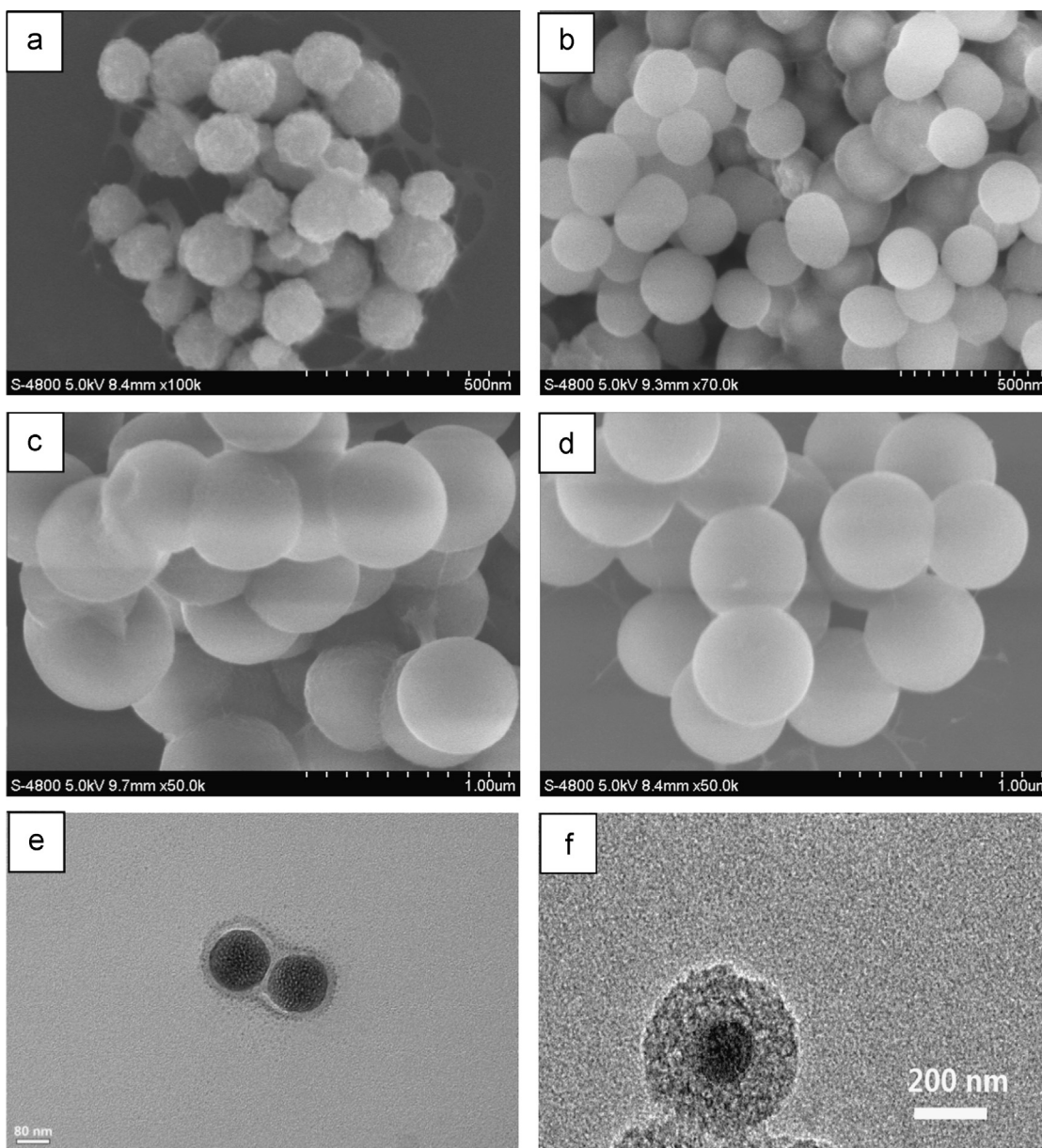


Fig. 1. SEM images of Fe₃O₄ nanoparticles (a), SiO₂@Fe₃O₄ (b) and MCM-41@Fe₃O₄ (c) and CDU-MCM-41@Fe₃O₄ (d), along with TEM image of SiO₂@Fe₃O₄ (e) and MCM-41@Fe₃O₄ (f).

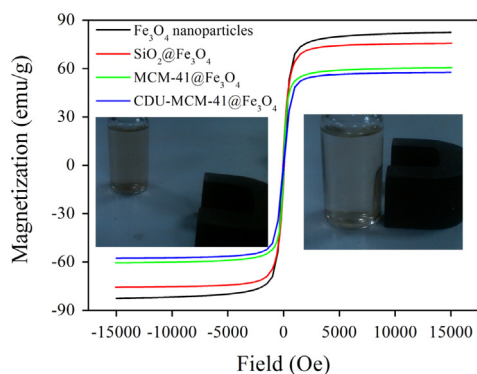


Fig. 2. Hysteresis loops of Fe_3O_4 nanoparticles, $\text{SiO}_2@\text{Fe}_3\text{O}_4$, $\text{MCM-41}@\text{Fe}_3\text{O}_4$ and $\text{CDU-MCM-41}@\text{Fe}_3\text{O}_4$. Inset (left): $\text{CDU-MCM-41}@\text{Fe}_3\text{O}_4$ suspension (10 mg in 50 mL of ethanol) without external magnetic field. Inset (right): $\text{CDU-MCM-41}@\text{Fe}_3\text{O}_4$ suspension (10 mg in 50 mL of ethanol) with external magnetic field.

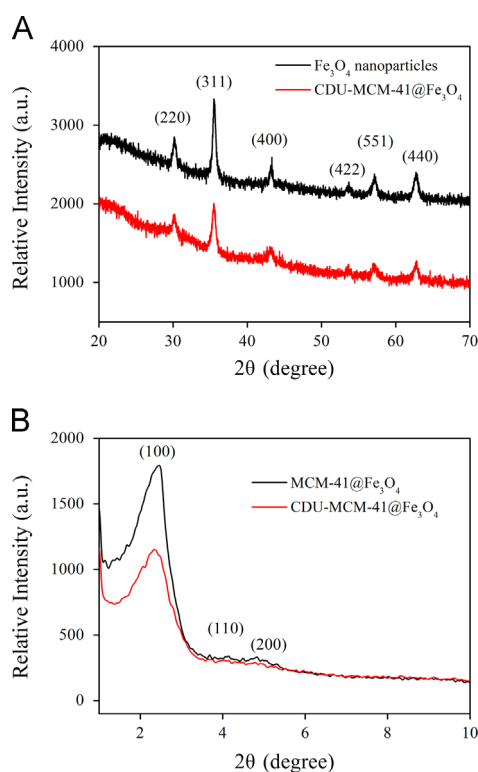


Fig. 3. (A) Wide-angle XRD patterns of Fe_3O_4 nanoparticles and $\text{CDU-MCM-41}@\text{Fe}_3\text{O}_4$. (B) SAXRD patterns of $\text{MCM-41}@\text{Fe}_3\text{O}_4$ and $\text{CDU-MCM-41}@\text{Fe}_3\text{O}_4$.

3.1.3. XRD patterns and N_2 adsorption/desorption

Wide-angle XRD patterns of Fe_3O_4 nanoparticles and $\text{CDU-MCM-41}@\text{Fe}_3\text{O}_4$ are presented in Fig. 3A for comparison. Despite their different intensity values, the two curves own nearly identical diffraction peaks indexed as (2 2 0), (3 1 1), (4 0 0), (4 2 2), (5 5 1) and (4 4 0), respectively, which is consistent with literature reports on Fe_3O_4 nanoparticles [14,16]. It is thus confirmed that there exists Fe_3O_4 magnetic core in $\text{CDU-MCM-41}@\text{Fe}_3\text{O}_4$ which has been well preserved after a series of modification procedures. Small-angle XRD (SAXRD) patterns of $\text{MCM-41}@\text{Fe}_3\text{O}_4$ and $\text{CDU-MCM-41}@\text{Fe}_3\text{O}_4$ are shown in Fig. 3B for comparison. A strong Bragg reflection peak and two weak ones which can be indexed as (1 0 0), (1 1 0) and (2 0 0) can be observed from both samples, suggesting that there is mesostructure on their surface [14,16,17]. Their intensity difference can be attributed to probe loading

procedure which partially compromised this highly ordered structure.

N_2 adsorption/desorption measurement is performed on $\text{MCM-41}@\text{Fe}_3\text{O}_4$ and $\text{CDU-MCM-41}@\text{Fe}_3\text{O}_4$ so that the mesostructure on their surface can be analyzed in detail. Their adsorption/desorption isotherms are typical IV-type ones (see Fig. S1, Supporting information), confirming that there is a mesostructure in $\text{MCM-41}@\text{Fe}_3\text{O}_4$ and $\text{CDU-MCM-41}@\text{Fe}_3\text{O}_4$ [16,17]. This mesostructure has been well preserved after light switch encapsulation. As for $\text{MCM-41}@\text{Fe}_3\text{O}_4$, its pore size, pore volume and BET surface area are 2.7 nm, 0.462 cm^3/g and 676.4 m^2/g , respectively, which are comparable to literature values [16,17]. After light switch loading procedure, these values decrease to 2.3 nm, 0.259 cm^3/g and 457.4 m^2/g respectively, suggesting that these light switch molecules have been successfully loaded into MCM-41 tunnels. This large porous structure can readily load cargo molecules, such as antitumor medicament.

3.1.4. IR spectra and TGA data

Covalent grafting between light switch and supporting host can be further confirmed by IR spectral analysis. IR spectra of CDU, $\text{MCM-41}@\text{Fe}_3\text{O}_4$ and $\text{CDU-MCM-41}@\text{Fe}_3\text{O}_4$ are shown in Fig. 4. As for IR spectra of $\text{MCM-41}@\text{Fe}_3\text{O}_4$ and $\text{CDU-MCM-41}@\text{Fe}_3\text{O}_4$, a series of bands peaking at 516 cm^{-1} , 753 cm^{-1} and 860 cm^{-1} , respectively, can be attributed to Si–O asymmetric stretching vibration, Si–O symmetric stretching vibration and Si–O–Si plane bending vibration, respectively [17], suggesting the successful formation of silica shell and MCM-41 tunnels in these samples. As for light switch CDU, a series of bands ranging from 2870 to 2980 cm^{-1} can be attributed to vibration of $-(\text{CH}_2)_3-$ group [17]. There is no $\text{N}=\text{C}=\text{O}$ stretch vibration ranging from 2250 to 2275 cm^{-1} , suggesting that CBD had completely reacted with TESPIC. The characteristic band peaking at 1645 cm^{-1} can be attributed to stretching vibrations of $\text{C}=\text{N}$ bond. The intense absorption bands peaking at 957 cm^{-1} , 1086 cm^{-1} and 1558 cm^{-1} , respectively, can be attributed to stretching vibrations of Si–O and Si–O bonds. The appearance of CDU $-(\text{CH}_2)_3-$ characteristic bands (2850 to 2968 cm^{-1}) in $\text{CDU-MCM-41}@\text{Fe}_3\text{O}_4$ IR spectrum indicates that light switch CDU has been immobilized in $\text{MCM-41}@\text{Fe}_3\text{O}_4$ tunnels. In addition, its red shift suggests that the covalent grafting decreases vibration frequencies. Some other characteristic bands, including $\text{C}=\text{N}$

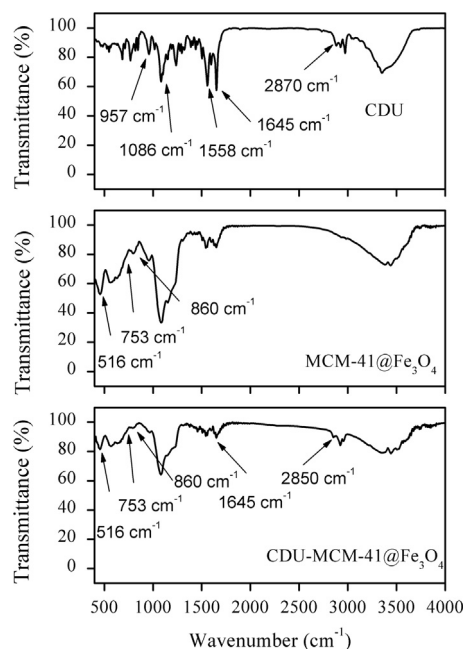


Fig. 4. IR spectra of CDU, $\text{MCM-41}@\text{Fe}_3\text{O}_4$ and $\text{CDU-MCM-41}@\text{Fe}_3\text{O}_4$.

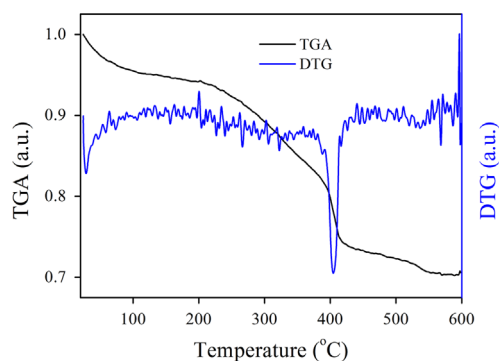


Fig. 5. TGA and DTG curves of CDU-MCM-41@Fe₃O₄.

bond (1645 cm^{-1}), Si–O and Si–O bonds (957 cm^{-1} , 1086 cm^{-1} and 1558 cm^{-1}), can be traced in CDU-MCM-41@Fe₃O₄ IR spectrum. However, more evidences are needed to say that CDU has been covalently grafted into MCM-41 tunnels. Their covalent grafting will be further proved below.

Light switch loading content in CDU-MCM-41@Fe₃O₄ is then determined by thermogravimetric analysis (TGA). Its TGA curve shown in Fig. 5 is composed of four major parts. The first one ranging from 25 to 188 °C is responsible for 6% weight loss and can be attributed to thermal release of organic solvents and physisorbed water molecules. The second one ranging from 210 to 380 °C and the third one ranging from 380 to 420 °C are totally responsible for 19.8% weight loss. Considering their sharp endothermic peaking at 404 °C, these two regions can be attributed to thermal breakdown and decomposition of light switch CDU. In other words, CDU loading content in CDU-MCM-41@Fe₃O₄ is as high as 19.8% which is slightly higher than literature values [14–17]. We attribute this improved loading content to the long MCM-41 tunnels in CDU-MCM-41@Fe₃O₄, as mentioned in Section 3.1.2. As for the last one ranging from 420 to 575 °C, it is responsible for 3.3% weight loss and can be assigned to thermal degradation and deconstruction of organosilicate framework in CDU-MCM-41@Fe₃O₄, such as Si–C, C–C and C–N bonds cleavage. For comparison, TGA and DTG curves of CDU and MCM-41@Fe₃O₄ are compared (see Figs. S2 and S3, Supporting information). As for pure CDU, its thermal decomposition temperature is much lower than that of CDU-MCM-41@Fe₃O₄, with three major endothermic peaks (236 °C, 264 °C and 443 °C). MCM-41@Fe₃O₄ is thermally stable with slim weight loss, no obvious endothermic peak is observed. This result confirms that CDU has been covalently grafted into MCM-41 tunnels and our composite is not the mixture of reactants.

3.2. Photophysical measurement on CDU-MCM-41@Fe₃O₄

We have above mentioned that light switch CDU is anticipated to be triggered by low energy light. Photophysical characters of CDU and CDU-MCM-41@Fe₃O₄ thus should be understood. Fig. 6 shows UV–vis absorption (abs.) and PL emission (em.) of CDU (1 μM in ethanol) and CDU-MCM-41@Fe₃O₄ (10 mg in 50 mL of ethanol), along with those of MCM-41@Fe₃O₄ (10 mg in 50 mL of ethanol) for comparison. CDU absorption spectrum is composed of a high energy absorption part and a low energy absorption part. The former one ranging from 220 to 370 nm can be attributed to $\pi \rightarrow \pi^*$ absorption of aromatic rings in CDU, with multiple peaks of 241 nm, 262 nm and 313 nm [15]. The latter one ranging from 390 to 620 nm is a broad one peaking at 510 nm and can be assigned to $\pi \rightarrow \pi^*$ absorption of C=N bond [15]. This C=N absorption is red shifted compared to literature reports based on N=N bond ($\lambda_{\text{abs}}=450\text{ nm}$), which makes low energy excitation of light switch

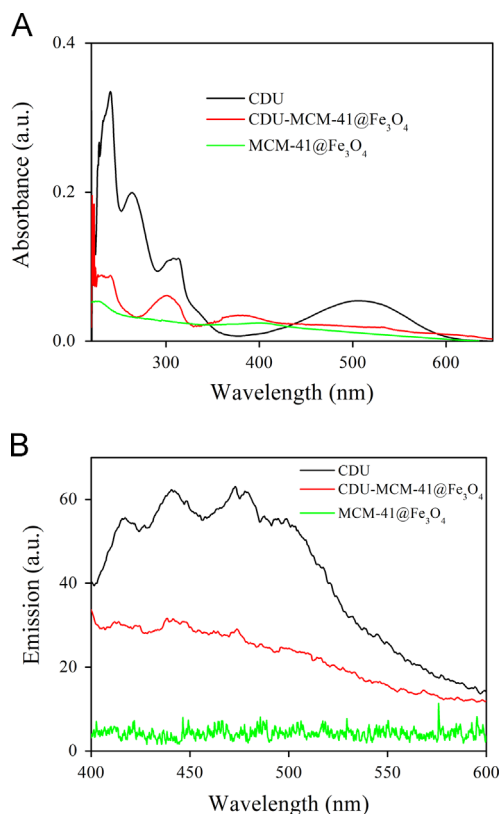


Fig. 6. (A) UV–vis absorption spectra of CDU (1 μM in ethanol), CDU-MCM-41@Fe₃O₄ (10 mg in 50 mL of ethanol) and MCM-41@Fe₃O₄ (10 mg in 50 mL of ethanol). (B) Low temperature (77 K) emission spectra of CDU (1 μM in ethanol), CDU-MCM-41@Fe₃O₄ (10 mg in 50 mL of ethanol) and MCM-41@Fe₃O₄ (10 mg in 50 mL of ethanol).

possible [14]. After being grafted into MCM-41 tunnels, these absorption peaks have been well preserved. As for the high energy absorption band, a slight blue shift tendency can be observed, which should be attributed to CDU interaction with silica framework. The low energy absorption band is widened, covering nearly whole visible region, suggesting that the light switch in CDU-MCM-41@Fe₃O₄ may be activated over a wide range from 400 to 600 nm. Upon various excitation wavelengths of 260 nm, 350 nm, 400 nm and 500 nm, no obvious emission signals can be observed from CDU and CDU-MCM-41@Fe₃O₄ at room temperature (see Fig. S4, Supporting information). Even when they are cooled to 77 K, only quite weak emission signals can be detected, as shown in Fig. 6. This fact suggests that all absorbed energy has been totally exhausted by *trans/cis* iso-merization of light-switch. An efficient *trans/cis* iso-merization motion can thus be expected for light stimulated release.

3.3. Controllable release performance of CDU-MCM-41@Fe₃O₄

Rhodamine 6 G was loaded into CDU-MCM-41@Fe₃O₄ so that its controllable release performance can be determined. Here, rhodamine 6 G was selected as cargo owing to its characteristic spectrum. As shown in Fig. 7, rhodamine 6 G emission peaking at 540 nm obviously increases upon light stimulus “on” state. Given light stimulus “off” state, rhodamine 6 G emission intensity is greatly maintained or even constant. There can be find a positive correlation between rhodamine 6 G emission intensity and light “on” state during above periodically varying light stimuli. It can thus be confirmed that CDU-MCM-41@Fe₃O₄ cargo release can be controlled by light stimuli. In other words, controllable cargo

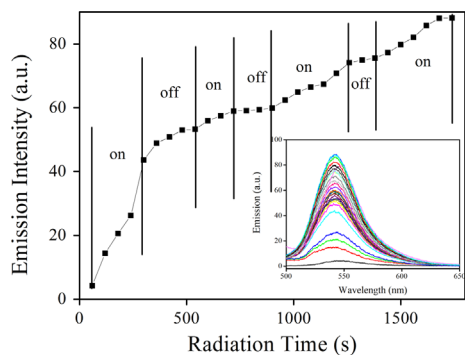


Fig. 7. Emission intensity monitoring ($\lambda_{em}=540$ nm) of CDU-MCM-41@Fe₃O₄ (10 mg in 50 mL of ethanol) loaded with rhodamine 6 G upon periodically changed light stimuli ($\lambda_{ex}=510$ nm), on and off. Inset: corresponding emission spectra.

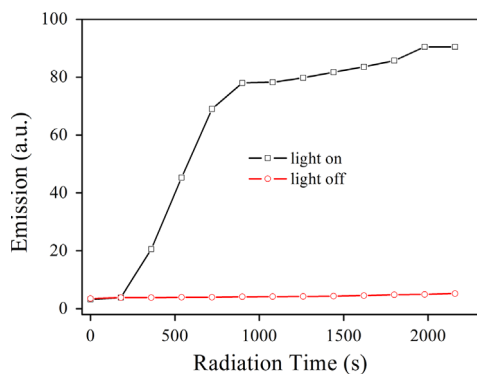


Fig. 8. Cargo holding and release performance of CDU-MCM-41@Fe₃O₄ under continuous light “on” and “off” states.

release from CDU-MCM-41@Fe₃O₄ has been realized with the help from light switch CDU.

Cargo holding and release performance of CDU-MCM-41@Fe₃O₄ under continuous light “on” and “off” states is analyzed as follows. As shown in Fig. 8, under darkness environment, rhodamine 6 G emission intensity remains constant at a low level, suggesting that few rhodamine 6 G molecules have been released. When exposed to continuous light excitation, rhodamine 6 G emission intensity increases sharply in the first 900 s, suggesting that most cargo molecules have been released during this time. Then the release procedure is greatly slowed, showing smooth release process. The whole release process can be finished in 2200 s. Compared to literature reports on similar core-shell structured site-specific delivery systems and biodegradable polymers, this release time seems to be long [14,18]. However, CDU-MCM-41@Fe₃O₄ can finish nearly 90% of its total capacity within 900 s, which makes it promising for further application. Here, this site-specific delivery system with magnetism-guiding and controllable release has been fully confirmed and characterized.

In order to further confirm this controllable release performance, emission monitoring of rhodamine 6 G, MCM-41@Fe₃O₄ and the mixture of CDU and MCM-41@Fe₃O₄ is recorded under continuous radiation and continuous darkness (see Supporting information, Figs. S5–S8). None of these components alone could respond to light stimuli. This fact confirms that CDU-MCM-41@Fe₃O₄ responds to light stimuli owing to the covalent combination of CDU and MCM-41@Fe₃O₄: only the light switch immobilized in MCM-41 tunnels could control and accelerate cargo

release, while light switch localized outside of MCM-41 tunnels is powerless to do so.

4. Conclusion

To sum up, a core-shell structured site-specific delivery system CDU-MCM-41@Fe₃O₄ was constructed with supermagnetic Fe₃O₄ as the core and mesoporous silica molecular sieve MCM-41 as the shell. A light switch CDU which could be triggered by low energy light was covalently grafted into MCM-41 hexagonal tunnels, serving as light stimuli acceptor. CDU-MCM-41@Fe₃O₄ was identified and confirmed by SEM, TEM, XRD patterns, N₂ adsorption/desorption, TGA, IR, UV-vis absorption and emission spectra. Experimental data suggested that CDU-MCM-41@Fe₃O₄ owned supermagnetic feature, which allowed its homogenous dispersion in aqueous solutions under no external magnetic field and site specific guiding under external magnetic field. Its hexagonal tunnels were as long as 180 nm, favoring cargo capacity improvement. Our light switch CDU was superior to literature ones by the fact that it could be excited by low energy light ($\lambda=510$ nm). Controllable release measurement on CDU-MCM-41@Fe₃O₄ suggested that CDU could effectively release its cargo molecules upon light stimuli with short release time of 900 s (90% capacity). These factors suggested that CDU-MCM-41@Fe₃O₄ could be further developed for magnetism-guiding site-specific delivery. For further improvements, real drug molecules should be tested. In addition, its size should be decreased for biological applications.

Acknowledgments

The authors thank our universities for financial supports.

Appendix A. Supporting information

Supplementary data associated with this article can be found in the online version at <http://dx.doi.org/10.1016/j.jssc.2015.02.019>.

References

- [1] M.E. Calderera-Moore, W.B. Liechty, N.A. Peppas, *Acc. Chem. Res.* **44** (2011) 1061–1070.
- [2] E.A. Rozhkova, *Adv. Mater.* **23** (2011) H136–H150.
- [3] I.I. Slowing, B.G. Trewyn, S. Giri, V.S.Y. Lin, *Adv. Funct. Mater.* **17** (2007) 1225–1236.
- [4] Q. Yuan, Y.F. Zhang, T. Chen, D.Q. Lu, Z.L. Zhao, X.B. Zhang, Z.X. Li, C.H. Yan, W.H. Tan, *ACS Nano* **6** (2012) 6337–6344.
- [5] Y. Deng, Y. Cai, Z. Sun, D. Zhao, *Chem. Phys. Lett.* **510** (2011) 1–13.
- [6] S.L. Gai, P.P. Yang, C.X. Li, W.X. Wang, Y.L. Dai, N. Niu, J. Lin, *Adv. Funct. Mater.* **20** (2010) 1166–1172.
- [7] J. Liu, S.Z. Qiao, Q.H. Hu, G.Q. Lu, *Small* **7** (2011) 425–443.
- [8] X. Liang, X. Li, L. Jing, X. Yue, Z. Dai, *Biomaterials* **35** (2014) 6379–6388.
- [9] Y. Zhu, T. Ikoma, N. Hanagata, S. Kaskel, *Small* **6** (2010) 471–478.
- [10] R. de la Rica, D. Aili, M.M. Stevens, *Adv. Drug Delivery Rev.* **64** (2012) 967–978.
- [11] J. Croissant, J.I. Zink, *J. Am. Chem. Soc.* **134** (2012) 7628–7631.
- [12] P. Yang, S. Gai, J. Lin, *Chem. Soc. Rev.* **41** (2012) 3679–3698.
- [13] Y. Wen, L. Xu, W. Wang, D. Wang, H. Du, X. Zhang, *Nanoscale* **4** (2012) 4473–4476.
- [14] Y. Wang, B. Li, L. Zhang, H. Song, L. Zhang, *ACS Appl. Mater. Interfaces* **5** (2013) 11–15.
- [15] L. Zhang, S. Yue, B. Li, D. Fan, *Inorg. Chim. Acta* **384** (2012) 225–232.
- [16] Y.Y. Wang, B. Li, L.M. Zhang, P. Li, L.L. Wang, J. Zhang, *Langmuir* **28** (2012) 1657–1662.
- [17] B. Lei, B. Li, H. Zhang, S. Lu, Z. Zheng, W. Li, Y. Wang, *Adv. Funct. Mater.* **16** (2006) 1883–1891.
- [18] M. Chen, D. Zhang, M.H. Xu, S.Q. Zhao, C.X. Sun, *Opt. Mater.* **36** (2013) 321–327.